COMPARISON OF TWO SEPARATION MULTIPATH TECHNIQUES IN GNSS REFLECTOMETRY FOR SEA LEVEL DETERMINATION IN INDONESIA

Lisa A. CAHYANINGTYAS[1] 🆔 *, Dudy D. WIJAYA[1]** 🆔 *, Nabila S.E. PUTRI[2]* 🆔

ABSTRACT:
GNSS reflectometry (GNSS-R) is a method to derive sea level using Signal to Noise Ratio (SNR) from the Global Navigation Satellite Systems (GNSS). SNR data consist of the direct signal from the satellite (multipath) and of the signals reflected by the sea surface, and hence separating the multipath is necessary to extract the signal from the sea surface. The process of separating multipath may affect the number of data and may eventually affect the quality of the derived sea level values. There are two multipath separation techniques that are mostly used: polynomial fitting and wavelet decomposition. This study investigates the performance of both techniques by applying them to analyze three months of the L1 SNR data of Global Positioning System (GPS) and Globalnaya Navigatsionnaya Sputnikovaya Sistema (GLONASS) as observed from two stations, Barus (CBRS) at North Sumatera from January 1 to March 31, 2022, and Morotai (CMOR) at North Maluku, Indonesia using data from February 1 to May 1, 2022. Comparison with sea level from tide gauge observations shows a high correlation for both techniques, with correlation coefficients of approximately 0.90 and 0.97 for CBRS and CMOR, respectively. The Root Mean Square Error (RMSE) of polynomial fitting for CBRS and CMOR have the same value, 11.5 cm, whereas those of wavelet are 11.4 cm and 11.5 cm. Since polynomial fitting and wavelet decomposition show similar performance, we conclude that both techniques give comparable accuracy of multipath SNR data for GNSS-R in Indonesia with appropriate quality control parameters.

Keywords: GNSS reflectometry, multipath, polynomial fitting, wavelet analysis, sea level.

1. INTRODUCTION

Multipath or reflected signals are one of the major error sources in high accuracy Global Navigation Satellite System (GNSS) positioning and numerous studies have presented multiple ways to mitigate the effects (Georgiadou and Kleusberg, 1987; Bilich et al., 2008). In contrast, Martin-Neira (1993) introduced the use of reflected GNSS signals for environmental sensing. Since then, various research related to the so-called GNSS reflectometry (GNSS-R), have been carried out to measure sea level (Anderson, 1999; Lofgren et al., 2011), snow depth (Larson et al., 2009), soil moisture (Chew et al., 2014), and vegetation water content (Wan et al., 2015). In terms of measuring sea level, GNSS-R has the advantage of allowing sea level observations to refer to a geocentric frame (Peng et al., 2021); reaching a large area rather than a single point (Roussel et al., 2014; Wang et al., 2018a); and being installed at a safe height on land to avoid extreme conditions in coastal areas (Peng et al., 2019). Anderson (1999) introduced the signal-to-noise ratio (SNR) to investigate interference patterns of the reflected GNSS signals. The SNR data were then exploited by Bilich and Larson (2007) for mapping the GNSS multipath on the reflected surface. To take advantage of the SNR data, the multipath frequency is usually separated using polynomial fitting (Larson et al., 2013; Lofgren, 2014).

Low-order polynomials are applied to extract multipath frequencies from the SNR data by removing the direct signal trend (Larson et al., 2008). Another method for separating multipath frequency is wavelet analysis, which is used in some SNR research. Bilich and Larson (2007) used wavelet analysis to extract the time-varying amplitude and frequency content of each signal. Wavelet analysis was also used by Wang et al. (2018b) to extract instantaneous Global Positioning System

---
[1] *Geodesy Research Group, Faculty of Earth Science and Technology, Bandung Institute of Technology, Jl. Ganesha 10, Bandung, Indonesia 40132, lisaayuc@gmail.com, *Corresponding author dudy.wijaya@itb.ac.id*
[2] *Surveying and Cadastre Research Group, Faculty of Earth Science and Technology, Bandung Institute of Technology, Jl. Ganesha 10, Bandung, Indonesia 40132, nabila.sofia@office.itb.ac.id*

(GPS) L1 SNR data and it significantly improves the time resolution but introduce additional outliers and errors. Wang et al. (2019) applied wavelet analysis to reduce noise using coherent superposition in multifrequency GNSS signals and the considerable improvements in data utilization and RMSEs can be achieved. Other study shows that applying wavelet decomposition can improve retrieval accuracy (Chen et al., 2019; Wang et al., 2018). It has been found that wavelet analysis if the following conditions surrounding the GNSS station hold: a narrow reflecting sensing zone, a small sea azimuth range, and fewer satellites over the GNSS station (Wang et al., 2019).

In this paper, we briefly summarize the results from our assessments on the performance of polynomial fitting and wavelet decomposition techniques in separating the multipath signals and in deriving the sea level values at some GNSS stations in Indonesia. After briefly mentioning the data and method (Section 2) used in our study, we analyze and discuss all numerical results (Section 3). Some remarks and conclusions are presented in Section 4.

2. DATA AND METHODS

2.1 Data and site description

We used three months of the SNR data of GPS and GLONASS (Globalnaya Navigatsionnaya Sputnikovaya Sistema) satellites as observed from two stations: Barus (CBRS) at North Sumatera (January 1-March 31, 2022) and Morotai (CMOR) at North Maluku, Indonesia (February 1-May 1, 2022). The three months data were used to get the sea level variations during neap tide and spring tide. The observation data were sampled every 30 seconds using right-handed circularly polarized (RHCP) geodetic antenna TRM159900 and Trimble Alloy receiver at both stations. We extracted the L1 SNR data by analyzing the S1 variable written in the GNSS RINEX (Receiver Independent Exchange format) files. CMOR and CBRS stations are co-located with continuous tide gauges measurements, with one hour sampling rate. Satellite observation documents in RINEX format and detailed satellite orbit information were then processed using the FORTRAN90 program (developed by our group) to extract the SNR data. Broadcast ephemeris data were used to determine the reflected plane above the sea surface and the direction of the plane. MATLAB programs developed by Roesler & Larson (2018) were modified to analyze the SNR data and to visualize the results.

Fig. 1 shows the location of the two sites. CMOR is located in the southern part of Morotai Island, North Maluku (2°0'59.624" N, 128°16'49.386" E) and CBRS is located in the southern part of North Sumatra Province, at 2°0'18,053" N and 98°23'52.445" E).
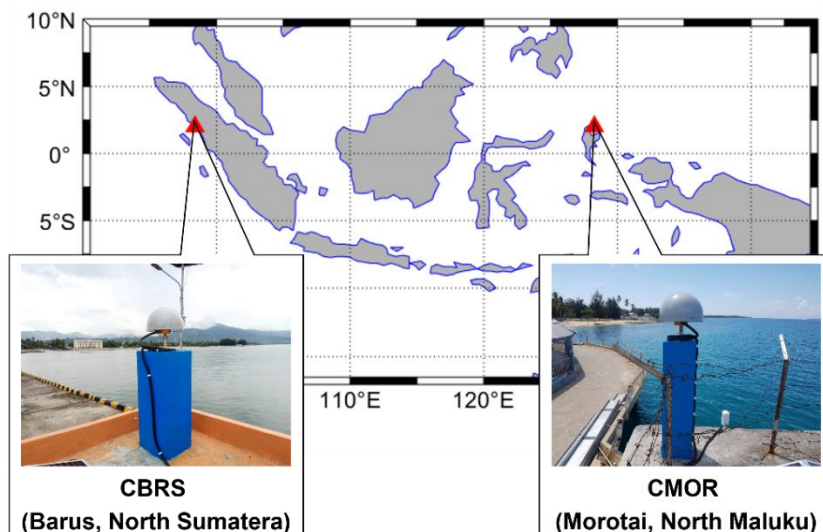

Fig. 1. Location of the two sites, CBRS and CMOR, and the view from the top of the tide station. Both stations are equipped with TRM159900 antenna and Trimble Alloy receiver.

2.2 SNR analysis method

As the satellite moves through space, the phase difference between the direct and multipath signals received by the receiver changes and then it creates an interference pattern. This interference pattern can be seen in the SNR data recorded by the receiver. Although the reflected signal will be suppressed by receiver gain on the geodetic antenna, data can still be obtained from satellites with low elevation angles (Larson et al., 2013; Lofgren, 2014; Wang et al., 2018b). Composite SNR due to the direct signal and reflected signal (multipath) can be defined using the law of cosine and geometric relations (Bilich et al., 2008; Larson and Nievinski, 2013; Lofgren, 2014; Wang et al., 2019):

$$SNR^2 = A_d^2 + A_m^2 + 2A_dA_m \cos\theta \tag{1}$$

the SNR in equation 1 is a function of the amplitude of the direct signal A_d, the amplitude of the multipath signal A_m, and the relative phase of the multipath θ.

The SNR data obtained from the measurement is the amplitude of the composite signal. By eliminating the contribution of signal errors, the SNR data for a single satellite and receiver observation can be modeled as follows (Larson et al., 2013; Lofgren and Haas, 2014; Roesler and Larson, 2018):

$$SNR(e) \approx A(e)\sin\left(\frac{4\pi H_R}{\lambda}\sin e + \phi\right) \tag{2}$$

where e is the elevation angle of the GNSS satellite relative to the horizon, $A(e)$ represents the amplitude of the SNR data, λ is the wavelength of the GNSS signal, ϕ is the phase difference, and H_R is the vertical distance between the antenna phase center and the surface of the horizontal reflecting plane (i.e. reflector height).

When the signal is received by the antenna, the receiver will record both the data from the direct signal and the reflected signal (i.e. the multipath). The geometry of the signal reflection will change as the satellite moves across the sky. This implies that the phase difference between the direct signal and the reflected signal changes, the SNR amplitude changes, and creates an interference pattern. By ignoring the phase effect of the antenna radiation pattern caused by the composition of the surface material and the plane of the planar reflection, the relative phase angle can be derived geometrically from the path delay δ of the reflected signal as (Larson and Nievinski, 2013; Lofgren, 2014; Wang et al., 2018a):

$$2\pi f = \frac{d\phi}{d\sin e} = 4\pi\frac{H_R}{\lambda} \tag{3}$$

where f and λ are the sinusoidal frequency and wavelength. This shows that under the condition of one ray reflection ϕ, the parameter has a linear relationship with $sin(e)$.

Equation 2 shows that the SNR observations has a sinusoidal relationship with the relative phase ϕ. Therefore, the SNR can be approximated by a sinusoidal relationship at a certain frequency. Using Equations (2) and (3), the reflector height can then be obtained:

$$H_R = \frac{\lambda f}{2} \tag{4}$$

The estimated reflector height over time can be obtained from the amplitude spectra of the irregular SNR data sample (Larson et al., 2009, 2013). Here, we employed the Lomb Scargle Periodogram (LSP) to analyze the power spectra of the SNR data, (Lomb, 1976; Scargle, 1982). The spectral power analysis of the SNR data as a function of the $sin(e)$ of the elevation angle enables the deriving of the multipath's dominant frequency (Lofgren and Haas, 2014).

2.2.1 Polynomial fitting

One of the most widely used multipath separation techniques in GNSS-R is polynomial fitting. Multipath separation using low-order polynomials (order 3–15) is suitable to analyze the SNR time series data (Bilich and Larson, 2007). Low-order polynomials were applied in the detrended SNR process to obtain multipath effects from the SNR data (Larson and Nievinski, 2013). The multipath effect of the SNR data will be used to obtain the reflector height. The SNR data units need to be converted into a linear scale from dB-Hz to volts/volts (Roesler and Larson, 2018; Geremia-Nievinski et al., 2020), using the equation 7:

$$SNR(dBHz) = 10 \log SNR \left(\frac{volts}{volts}\right)^2 \tag{5}$$

$$SNR(dBHz) = 20 \log SNR \left(\frac{volts}{volts}\right) \tag{6}$$

$$SNR \left(\frac{volts}{volts}\right) = 10^{\frac{SNR(dBHz)}{20}} \tag{7}$$

After being converted into linear units, the SNR data can be used in the detrending process to eliminate the trend of the direct signal. In this study, we accomplished some trials to find an optimal polynomial order used for the detrending process. We found that the fourth-order polynomial seems more appropriate than the second-order or third-order polynomial. For each satellite arc, these low-order polynomials are then used to remove the trend, creating a dSNR (detrended SNR or the composite SNR) arc. The dSNR represents the effect of the reflected signal on the SNR data, which consists of the multipath oscillations as written in Equation 8 (Zhou et al., 2019):

$$dSNR_{com} = SNR_{com} - \frac{P_d + P_r + P^I}{P_n} = A \cos \left(\frac{4\pi H_R \sin e}{\lambda} + \phi\right) \tag{8}$$

where A is the amplitude of the composite SNR. After extracting the direct SNR trend, it can get the multipath SNR by removing the direct SNR trend.

2.2.2 Wavelet analysis

Wavelet is used in the direct signal detrending process to obtain a multipath SNR with minimum noise (Wang et al., 2018a). The frequency component of the signal above sea level and the noise frequency can be separated using the wavelet decomposition. The accuracy of the GNSS-R sea level estimation data is improved by the wavelet decomposition (Chen et al., 2019). The wavelet decomposition is simply a technique that aids in splitting the original signal into its low-frequency and high-frequency components. It will also be possible to further separate the low-frequency part into its into lower-frequency and higher-frequency components.

The concept of wavelet was first introduced by Morlet in 1984. Under the guidance of Grossman, Morlet introduced the continuous wavelet transform (CWT), which is shown in equation 9 (Peng and Chu, 2004):

$$W_\psi f(m,n) = \langle f, \psi_{m,n} \rangle = m^{-1/2} \int_{-\infty}^{\infty} f(t) \bar{\psi} \left(\frac{t-n}{m}\right) dt \tag{9}$$

where m is the scale parameter, n is the time parameter, $\psi(t)$ is the wavelet analysis, and ($\bullet$) represents the complex conjugate of $\psi(\bullet)$. In the process of analyzing real data, the parameters must be made in discrete form (Chen et al., 2019). Daubechies and Mallat developed wavelet to analyze the continuous signals become discrete forms. To solve the discrete wavelet transform (DWT), Mallat (1989) proposed an approach that uses wavelet filters to decompose and reconstruct the signal. According to Mallat (1989), the decomposition algorithm is written as follows:

$$A_j[f(t)] = f(t) \tag{10}$$

$$A_x[f(t)] = \sum_y H(2t - k) A_{x-1}[f(t)] \tag{11}$$

$$D_x[f(t)] = \sum_y G(2t - k) A_{x-1}[f(t)] \tag{12}$$

where A_i is the amplitude of the decomposed signal, $t = 1, 2, . . . , N$ is a discrete serial time number, N denotes the signal length, represents the original signal, $m = 1, 2, . . . , M$ represents the decomposition level and M represents the maximum decomposition level, H and G are the low-frequency and high-frequency wavelets that pass through the decomposition filter, and are the wavelet coefficients of at the low and high frequencies of the *M*-level.

The SNR data, as previously explained, are composite signals of SNR data, which are the sum of the direct and multipath signal strengths. By subtracting the composite signal from the decomposed low-frequency signal, the multipath effect of wavelet decomposition is obtained. In this study, we used 8-level Daubechies 4 wavelet (db4) as a wavelet function to decompose and reconstruct the signal. Following the collection of multipath SNR data, an analysis process is carried out using LSP, as explained in the following section.

2.3 Validation

The accuracy and correlation between the GNSS-R and the tide gauges shall be used as the main indicators to assess the the quality of sea level values as derived by the GNSS-R. The root means square error (RMSE) value shows the accuracy, while the R-square value (R^2) represents the correlation between the two data sets. The RMSE value is calculated using equation 13:

$$RMSE = \sqrt{\sum_{i=1}^n \frac{(\widehat{y_i} - y_i)}{n}} \tag{13}$$

where $\widehat{y_i}$ is the sea level from GNSS-R, y_i represents the sea level from tide gauges, and n is the amount of data. The correlation coefficient, or r (see equation 14), is the square root of the comparison between the square of the difference between the GNSS-R data and the model and the square of the difference between the data and the GNSS-R data average.

$$r = \sqrt{R^2} = \sqrt{1 - \frac{\sum(y_i - \widehat{y_i})}{\sum(y_i - \overline{y_i})}} \tag{14}$$

where $\widehat{y_i}$ is the output of the GNSS-R data regression. When the resulting correlation coefficient value is close to 1, the correlation between the GNSS-R data results is strong. The correlation coefficient shows that the produced regression results may explain and show how close the data correlate to the obtained regression results.

In addition to examining the accuracy and correlation of the GNSS-R data with tide gauge, tidal constituents are calculated from the GNSS-R sea level height results at both stations. Because the GNSS-R sea level height data are not regularly sampled, the response method was used to obtain the tidal components (Munk and Cartwright, 1966). Tidal analysis using the response method was also applied to tide gauge data. The amplitude and phase values of the four main tidal constituents, S2, M2, K1, and O1, are compared in this study.

To compare the quality of GNSS-R and tide gauge sea level height measurements, the absolute error value is calculated. The absolute error value is calculated from the difference between GNSS-R and tide gauge amplitude and phase of the tidal components. Equation 17 were used to calculate the absolute error:

$$R_{amp} = \sqrt{A_1^2 + A_2^2 - 2A_1 A_2 \cos(\Phi_1 - \Phi_2)} \tag{15}$$

$$R_{phase} = arctan\left(\frac{A_2 sin\Phi_2 - A_1 sin\Phi_1}{A_2 cos\Phi_2 - A_1 cos\Phi_1}\right) \tag{16}$$

$$Error_{absolute} = R_{amp}.cos R_{phase} \tag{17}$$

where A_1 is the amplitude of tidal constituents from tide gauges, A_2 is the amplitude of tidal constituents calculated from GNSS-R data, Φ_1 is the phase of tidal constituents from tide gauges data, Φ_2 is the phase of tidal constituents from GNSS-R data, R_{amp} is the residual amplitude, R_{phase} is the residual phase. The absolute error was used to determine the total residuals from the tidal amplitude and phase values.

3. RESULTS AND DISCUSSIONS

3.1. GNSS signal reflection area

The GNSS satellite signals that reflect off the ocean's surface form an area rather than specular point. Assuming that the reflecting plane is planar, the reflected signal can be described by specifying the First Fresnel Zone (FFZ). The signal reflection area above sea level was determined using the FFZ data to investigate the study area (Roussel et al., 2014; Geremia-Nievinski et al., 2016). The coverage area of the reflected plane may be seen using the FFZ position mapping, which also aids in calculating the optimal elevation and azimuth angle for each study site. According to the FFZ data, the Fresnel zone becomes smaller as satellite height increases. As the satellite height rises, the multipath impact diminishes, which is exactly proportional to it.

The FFZ at CBRS and CMOR are generated by using 6 m reflected height, with respect to the sea surface. **Fig. 2** shows the reflected signal at CBRS and CMOR as a 2D ellipse shape of the FFZ. Yellow, dark blue, red, green, and cyan ellipses represent the reflected signal region from satellites with an elevation of 5°, 10°, 15°, 20°, and 25° elevation. In comparison to ellipses at other elevation angles, those at an elevation angle of 5° have the longest major axes. At elevation angle of more than 25°, the multipath no longer comes from the sea surface reflection plane. The mapping results of the FFZ are displayed in **Fig. 2**.
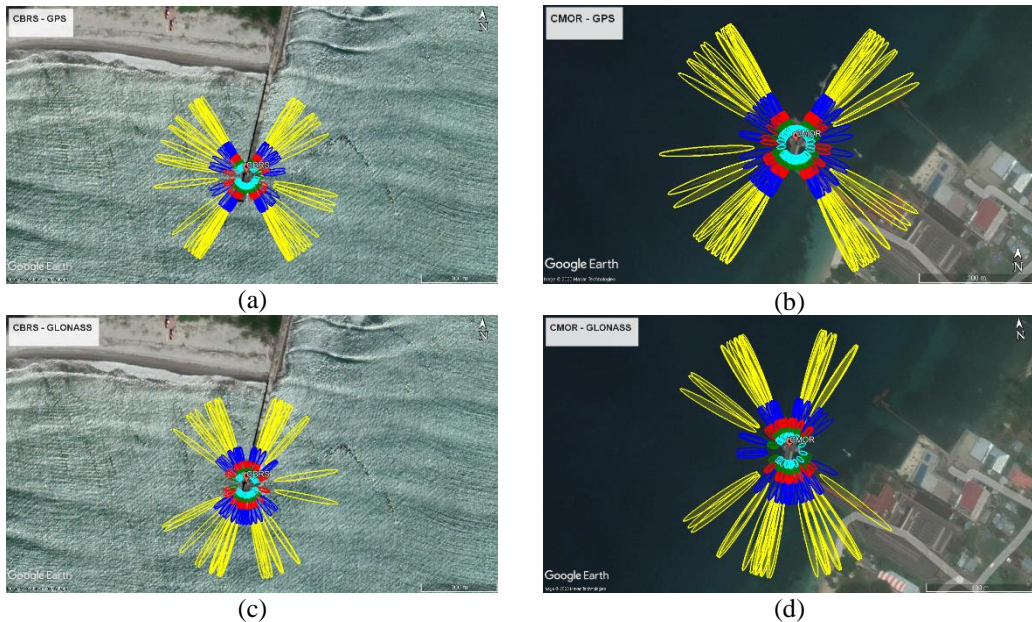

Fig. 2. The reflection areas were approximated by the FFZ at CBRS (a, c) and CMOR (b, d). The ellipses represent the reflected GPS L1 signals for elevation angles 5° (yellow), 10° (blue), 15° (red), 20° (green), and 25° (cyan). (Generated using https://github.com/kristinemlarson/gnssrefl).

All FFZ at CMOR are discovered to be above the sea surface reflection plane, as shown in **Fig. 2b and 2d** (right). Above the pier bridge, the reflected signal is visible as an ellipse at 25° elevation angle. This indicates that the reflected signal from the pier has been composited with the reflected signal at 25°. Based on Purnell et al. (2021), the reflector height measurements are generally less precise at elevation angles greater than 30°. The effect of random noise in SNR data leads to a greater uncertainty at larger elevation angles by using geodetic-standard antennas (Purnell et al., 2020). The reflected signal with an elevation angle above 25° is therefore not used in the following data processing.

According to the Fresnel zone mapping at CBRS, the multipath cannot be analyzed on the northern portions of the azimuths 350°-0° and 0°-30° since the Fresnel zone is on the pier bridge.

The Fresnel zone is also located above the pier bridge in the azimuth range of 160° to 208° in the southern section of the range, causing multipath from this region useless as well. Therefore, it is determined that CBRS uses reflected signals from the satellites with elevation angles of 5°-20° at azimuths of 30°-160° and 208°-350° based on the findings of FFZ visualization in **Fig. 2**. The area of the study based on the FFZ analysis can be seen in **Table 1**.

<div align="right">**Table 1.**</div>

<div align="center">**Area of the study including azimuth and elevation angle at CBRS and CMOR**</div>

Study area	CBRS	CMOR
Azimuth	30°-160° and 208°-350°	180°-360°
Elevation	5°-20°	5°-20°

3.2. Data analysis

As described in Section 2.2, multipath separation is accomplished by eliminating the direct signal. Detrending methods for signal processing, such as polynomial fitting or wavelet decomposition, can be used to determine the trends of direct signals. The detrended procedure is performed on each satellite arc, which is split into 30 epochs, meaning that every 15 minutes. The time span of satellite arc must be 15 minutes to compute frequencies up to the pseudo-Nyquist limit and get valid reflector height (Roesler & Larson, 2018). Detrending the polynomial fit is performed to obtain a trending direct signal. In addition, to get the multipath SNR value, the value of the combined SNR is lowered by the trend value of the direct signal derived from the detrending method.

Fig. 3 shows the results of multipath signal separation using polynomial fitting at CBRS and CMOR. The figure contains three components: the composite signal (green), the trend of the polynomial fitting (red), and the multipath (blue). A direct signal is indicated by the red line that shows the trend from polynomial fitting. **Fig. 3** shows that the direct signal increases as the elevation angle increases. The blue line depicting the multipath SNR is obtained by combining the SNR reduction with the trend value of the polynomial fitting, thus the results are unaffected by direct signal effects.
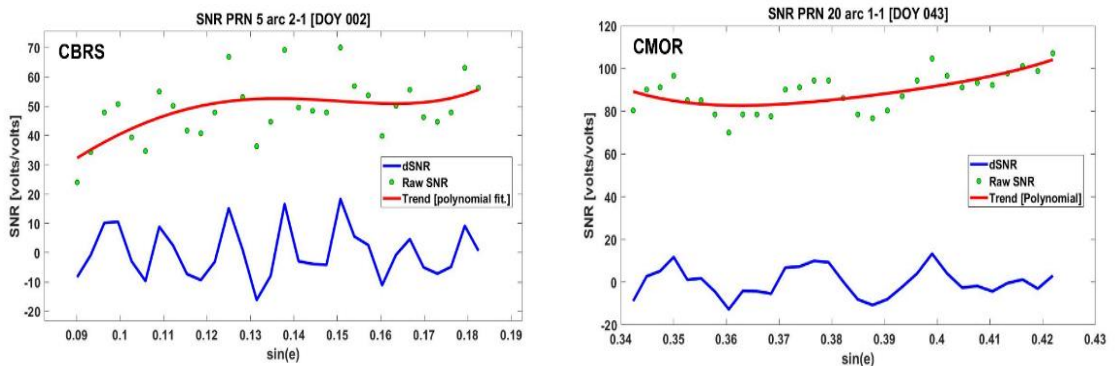

Fig. 3. Multipath separation using polynomial fitting. The green dots are the raw data of SNR from RINEX file. The red line is the trend of the SNR approached by 4th degree polynomial. The blue line is the detrended SNR.

In contrast to polynomial fitting, the signal detrending process in wavelet decomposition is performed to obtain the low-frequency trend of SNR data. By obtaining low frequencies (low wavelets) from the wavelet decomposition, multipath SNR values can be determined. The multipath SNR is determined by subtracting the composite and low-wavelet SNR. The low frequency of the wavelet decomposition results indicates a direct signal. Therefore, a reduction between the composite SNR and low-wavelet is performed to eliminate the direct signal effect, and a multipath SNR is obtained.

Fig. 4 depicts the detrended wavelet decomposition results from SNR data at CBRS and CMOR. Each image consists of three components: the composite signal, multipath, and low wavelet trend. Green dots represent the composite signal, which is also known as raw SNR. The blue line represents

the multipath result of wavelet decomposition, and the red line represents the trend of low wavelets. **Fig. 4** shows that the multipath SNR value of the decomposition results is approximately equal to the composite SNR, due to the signal scaling performed on the $sin(e)$. The low wavelet trend from the two stations, CBRS and CMOR, appears to be increasing as the elevation angle increases.
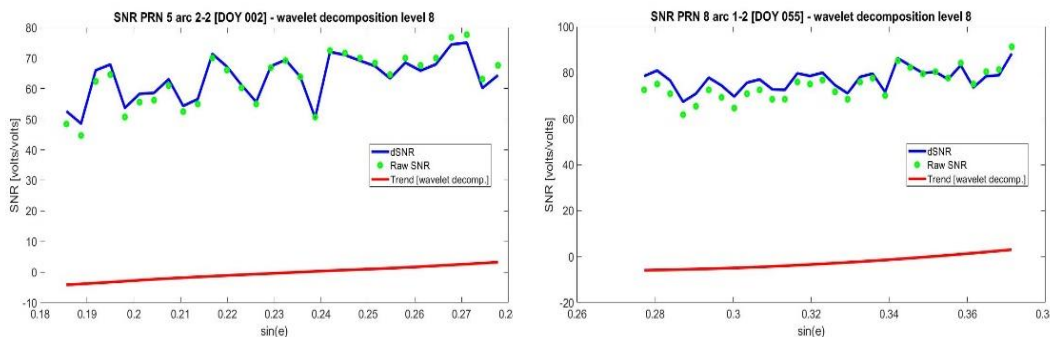

Fig. 4. Multipath separation using wavelet analysis. The green dots are the raw data of SNR from RINEX file. The red line is the trend of the SNR filtered using wavelet decomposition. The blue line is the detrended SNR.

The multipath SNR is processed with an LSP to obtain the reflector height. The LSP algorithm is used to generate the normalized spectral strength or periodogram from a set of SNR time series data for each predefined time range. To get an accurate reflector height, quality control is applied to the data from both stations during the LSP process by adjusting the peak-to-noise ratio (>2.4 for both stations), minimum amplitude (>4 for both stations), and reflector height (4-10 for both stations).

After the LSP analysis and quality control, sea level height was estimated from the separation results using polynomial fitting and wavelet analysis. The quality control is applied in the process, including the amplitude of the normalized spectrogram, peak-to-noise ratio, and range of the reflector height. **Fig. 5** show the sea level height from multipath separation technique using polynomial fitting (upper) and wavelet analysis (lower) at CBRS and CMOR. After applying the quality control, the number of observations obtained decreased.
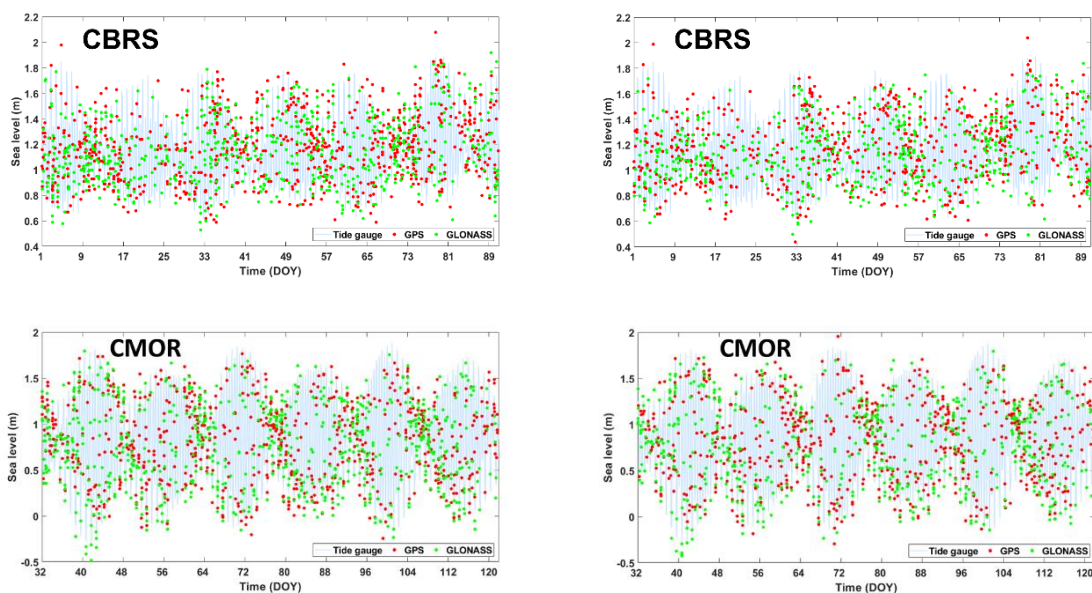

Fig. 5. The timeseries of sea level from GNSS-R (L1 GPS and GLONASS signals) using polynomial fitting (left) and wavelet analysis (right) for multipath separation at CBRS (upper) and CMOR (lower).

A significant amount of data is eliminated since it does not pass the specified threshold due to the usage of several parameters. The data collected at two stations from GNSS-R using all the methods of multipath separation are generally similar. However, by applying polynomial fitting at both stations, more data can be generated than by using wavelet analysis.

Initially, the reflector height obtained is that of the sea level relative to the antenna phase centre. The reflector height was corrected in this study by measuring the height difference between the zero tidal palm and the phase center antenna using precise levelling method. Therefore, GNSS-R and tide gauge data refer to the same reference sea level.

3.3. Comparison with co-located tide gauge

The results from the polynomial fitting and wavelet analysis on sea level height were then compared with tide gauge data. GNSS-R sea levels are irregularly sampled as it is displayed in **Fig. 5** and more data are obtained on the day with low tidal ranges. The residuals were calculated from the difference between sea level from GNSS-R and tide gauge at the time-tag of GNSS-R. Therefore, the hourly tide gauge data were interpolated to the GNSS-R time-tag. From the sea level at the same time-tag, the correlation between sea level from tide gauges and GNSSR are also calculated (see **Fig. 6**). **Table 2** summarizes the RMSE results and correlations at each station from the separation results using polynomial fitting (polyfit) and wavelet decomposition (waveldec) with tide gauge observations.
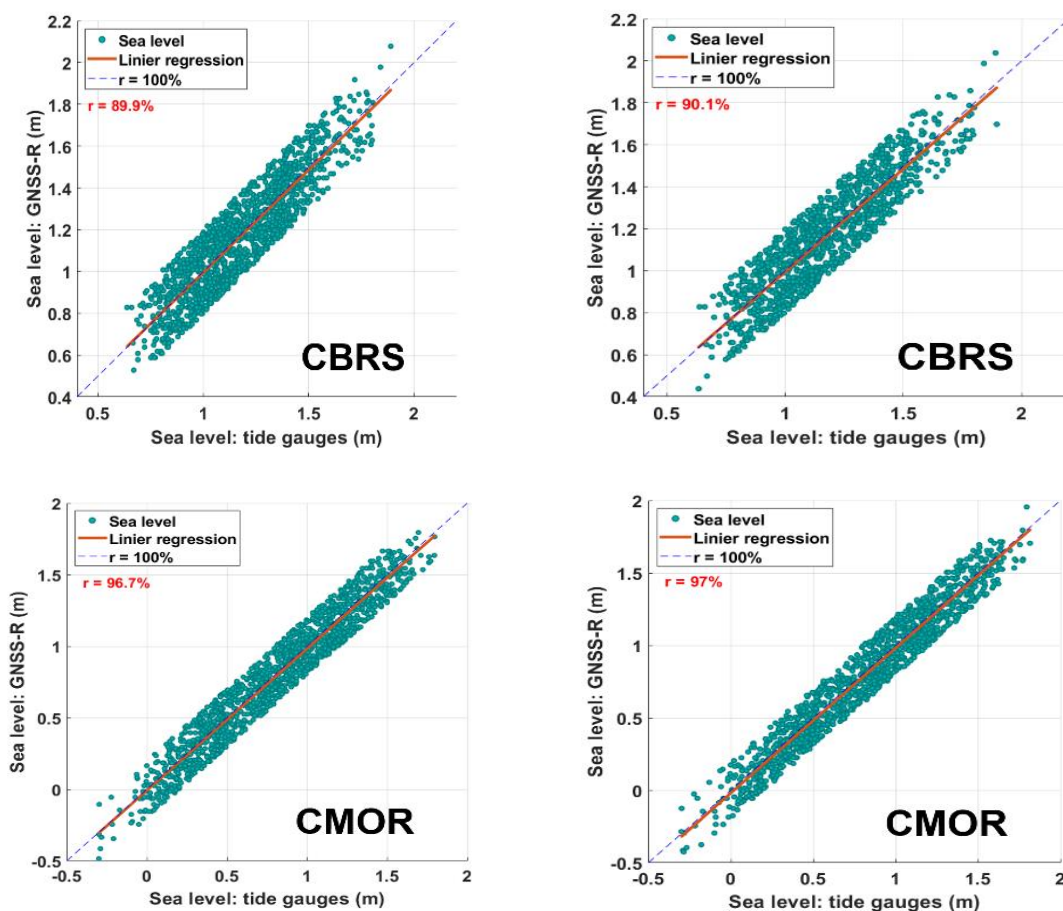

Fig. 6. The correlation between sea level from tide gauges and GNSSR using polynomial fitting (left) and wavelet analysis (right) for multipath separation at CBRS (upper) and CMOR (lower

RMSE, correlation with tide gauge, and the number of observations from GNSSR using polynomial fitting and wavelet analysis at CBRS and CMOR

Station	RMSE (cm)		Correlation (%)		Number of Observations	
	Polyfit	Waveldec	Polyfit	Waveldec	Polyfit	Waveldec
CBRS	11.5	11.4	89.9	90.1	1470	1235
CMOR	11.5	11.3	96.7	97	1525	1322

Based on the correlation value obtained by comparing the GNSS-R results with a tide gauge, the GNSS-R results using wavelet decomposition for multipath separation show slightly better results at both stations and higher correlation value. However, both stations have shown that multipath separation using polynomial fitting gets more measurement data than wavelet analysis.

Table 3 shows the summarize the amplitude and phase values of GNSS-R from polynomial fitting and GNSS-R from wavelet analysis at the CBRS. The response method tidal analysis results show a difference in the amplitude values of the M2 constituents. Figure 3.15 depicts the amplitude and phase values of the CMOR data. The three data sets used produced similar results for all tidal constituents (S2, M2, K1, and O1).

Table 3.
Tidal constituents from GNSS-R using polynomial fitting and wavelet decomposition at CBRS and CMOR.

Sta	S2		M2		K1		O1	
	Polyfit	**Waveldec**	**Polyfit**	**Waveldec**	**Polyfit**	**Waveldec**	**Polyfit**	**Waveldec**
Amplitude (m)								
CBRS	0.1040	0.1078	0.1565	0.1698	0.0812	0.0863	0.0574	0.0556
CMOR	0.2571	0.2551	0.5176	0.5208	0.1730	0.1732	0.1199	0.1179
Phase (°)								
CBRS	358.39	359.04	322.56	319.17	25.53	32.83	189.89	197.35
CMOR	306.83	307.71	283.35	283.46	262.50	261.73	74.53	75.71

Fig. 7 depicts the absolute error values at CBRS and CMOR stations. The errors at CBRS are obviously larger than those at CMOR.
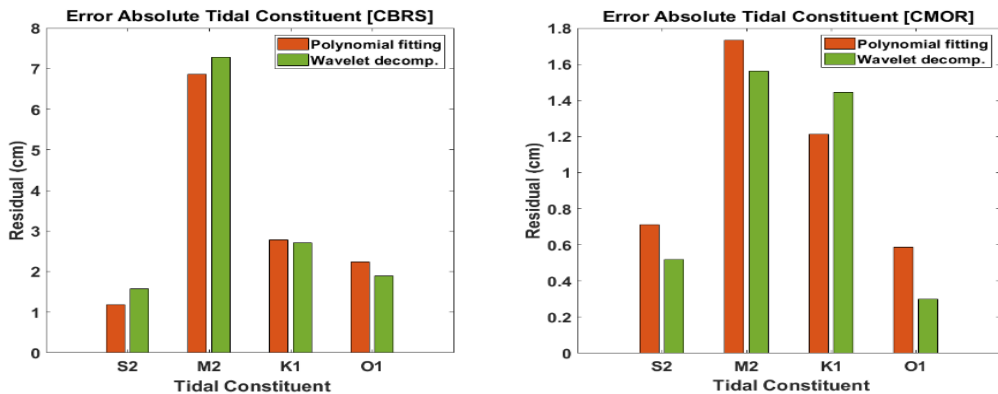

Fig. 7. Absolute error of tidal constituents at CBRS (left) and CMOR (right).

At CBRS station, the total value of the residual vector is almost the same for multipath separation using polynomial fitting and wavelet decomposition, namely between 1 cm to 7 cm. Both the GNSS-R polynomial fitting and the wavelet analysis show a significant difference of 7 cm in the M2. At CMOR station, the error of M2 is larger than that of another tidal constituent. This result suggests that the data from multipath separation using wavelet decomposition has a higher proximity value to tide gauge than the data from multipath separation using polynomial fitting.

The characteristics of the tides at the observation locations influence the difference in residual vector values from the two tidal stations in general. The number of observations obtained is also affected using quality control. The number of parameters used when processing with LSP yields a lot of unused data. On the other hand, the use of quality control parameters can result in data with high quality and reliability.

4. REMARKS AND CONCLUSION

In terms of determining sea level with GNSS-R, both multipath separation algorithms perform equally well. The sea level height results from the GNSS-R are in good agreement with those observed by the tidal gauges. The correlation value of the CBRS and CMOR using GNSS-R are respectively 90% and 96%, compared to the tidal gauges. These results indicate that the capability of the GNSS-R depends on the characteristics and environmental conditions nearby the station. During low tide range conditions, the two stations can produce more data. Despite a significant amount of data, the precision of the derived sea level height is not high; the RMSE for CBRS is 8.7 cm and 8.4–8.8 cm for CMOR. The station environment's wind speed is another aspect that affects the accuracy of the data obtained. Due to a lack of meteorological data near the observation site, the wind speed was not considered in this study. The roughness of the ocean is influenced by the velocity of the wind, which may violate the assumption of the planar sea surface.

The GNSS-R sea level results from the two multipath separation techniques are comparable. The implementation of the two techniques depends on the conditions at the observation area. By establishing a low order polynomial, the polynomial fitting technique is highly practical. On the other hand, to use wavelets, it is important to evaluate the proper wavelet family and order. The Wavelet decomposition is a technique for eliminating noise while preserving the frequency characteristics of the observed data. However, the wavelet decomposition is sensitive to noise. The process of multipath separation has a substantial effect on the quality of estimating sea level height from GNSS-R.

The quality of the sea level height results is also proven by the residual vector of the tidal constituents. The tidal characteristics at the observation locations impact the residual vector differences between the two tide stations. In addition, the total amount and density of the obtained data impact its accuracy. The implementation of quality control affects the amount of data obtained. The number of parameters applied during LSP processing causes a significant amount of unwanted data. However, using quality control settings can result in dependable and high-quality data.

GNSS-R sea level data derived from the two multipath separation techniques employed have RMSE values between 8-9 cm and a correlation of more than 90%. Based on these results, it is technically possible to apply polynomial fitting and wavelet as a multipath separating technique in GNSS-R. The quality of the data is influenced by quality control, the effect of rising and setting satellites, the tides at each station, the temporal resolution of the data obtained, and the characteristics and conditions of the study area.

The GNSS-R method for determining sea level height can be used to combine the existing tides data. In this study, the same quality control parameter values were applied throughout the process by using LSP to compare the sea level height from both methods. To achieve high-quality GNSS-R sea level estimates, LSP analysis for each multipath SNR data from polynomial fitting and wavelet decomposition is required. Observational data with high rate, multi frequencies and multi constellation satellites can be used to improve the temporal resolution of the data. The application of quality control to multipath SNRs resulting from the separation of polynomial fitting and wavelet decomposition can be identified because the resulting SNR series may be distinct.

ACKNOWLEDGEMENTS

R E F E R E N C E S

Anderson, K. D. (1999). Determination of Water Level and Tides Using Interferometric Observations of GPS Signals.

Bilich, A., & Larson, K. M. (2007). Mapping the GPS multipath environment using the signal-to-noise ratio (SNR). Radio Science, 42(6). https://doi.org/10.1029/2007RS003652

Bilich, A., Larson, K. M., & Axelrad, P. (2008). Modeling GPS phase multipath with SNR: Case study from the Salar de Uyuni, Boliva. Journal of Geophysical Research: Solid Earth, 113(4), 1–12. https://doi.org/10.1029/2007JB005194

Chen, F., Liu, L., & Guo, F. (2019). Sea Surface Height Estimation with Multi-GNSS and Wavelet De-noising. Scientific Reports, 9(1). https://doi.org/10.1038/s41598-019-51802-9

Chew, C. C., Small, E. E., Larson, K. M., & Zavorotny, V. U. (2014). Effects of near-surface soil moisture on GPS SNR data: Development of a retrieval algorithm for soil moisture. IEEE Transactions on Geoscience and Remote Sensing, 52(1), 537–543. https://doi.org/10.1109/TGRS.2013.2242332

Daubechies, I. (1990). The Wavelet Transform, Time-Frequency Localization and Signal Analysis. IEEE, 36, 961–1005.

Georgiadou, Y., & Kleusberg, A. (1987). On carrier signal multipath effects in relative gps positioning.pdf. Manuscripta Geodaetica, 13, 172–179.

Geremia-Nievinski, F., Hobiger, T., Haas, R., Liu, W., Strandberg, J., Tabibi, S., Vey, S., Wickert, J., & Williams, S. (2020). SNR-based GNSS reflectometry for coastal sea-level altimetry: results from the first IAG inter-comparison campaign. Journal of Geodesy, 94(8). https://doi.org/10.1007/s00190-020-01387-3

Geremia-Nievinski, F., Silva, M. F. E., Boniface, K., & Monico, J. F. G. (2016). GPS Diffractive Reflectometry: Footprint of a Coherent Radio Reflection Inferred from the Sensitivity Kernel of Multipath SNR. IEEE Journal of Selected Topics in Applied Earth Observations and Remote Sensing, 9(10), 4884–4891. https://doi.org/10.1109/JSTARS.2016.2579599

Larson, K. M., Gutmann, E. D., Zavorotny, V. U., Braun, J. J., Williams, M. W., & Nievinski, F. G. (2009). Can we measure snow depth with GPS receivers? Geophysical Research Letters, 36(17), 1–5. https://doi.org/10.1029/2009GL039430

Larson, K. M., Löfgren, J. S., & Haas, R. (2013). Coastal sea level measurements using a single geodetic GPS receiver. Advances in Space Research, 51(8), 1301–1310. https://doi.org/10.1016/j.asr.2012.04.017

Larson, K. M., & Nievinski, F. G. (2013). GPS snow sensing: Results from the EarthScope Plate Boundary Observatory. GPS Solutions, 17(1), 41–52. https://doi.org/10.1007/s10291-012-0259-7

Larson, K. M., Small, E. E., Gutmann, E. D., Bilich, A. L., Braun, J. J., & Zavorotny, V. U. (2008). Use of GPS receivers as a soil moisture network for water cycle studies. Geophysical Research Letters, 35(24), 1–5. https://doi.org/10.1029/2008GL036013

Löfgren, J. S., & Haas, R. (2014). Sea level measurements using multi-frequency GPS and GLONASS observations. Eurasip Journal on Advances in Signal Processing, 2014(1). https://doi.org/10.1186/1687-6180-2014-50

Löfgren, J. S., Haas, R., & Johansson, J. M. (2011). Monitoring coastal sea level using reflected GNSS signals. Advances in Space Research, 47(2), 213–220. https://doi.org/10.1016/j.asr.2010.08.015

Löfgren, J. S., & Haas, R. (2014). Sea level observations using multi-system GNSS reflectometry. Chalmers University of Technology.

Lomb, N. R. (1976). Least-squares frequency analysis of unequally spaced data. Astrophysics and Space Science, 39(2), 447–462. https://doi.org/10.1007/BF00648343

Mallat, S. G. (1989). A Theory for Multiresolution Signal Decomposition: The Wavelet Representation. In IEEE TRANSACTIONS ON PATTERN ANALYSIS AND MACHINE INTELLIGENCE: Vol. I (Issue 7).

Martin-Neira, M., Colmenarejo, P., Ruffini, G., & Serra, C. (2002). Altimetry precision of 1 cm over a pond using the wide-lane carrier phase of GPS reflected signals. Remote Sensing, 28(3), 394–403.

Munk, W.H., Cartwright, D.E., 1966. Tidal Spectroscopy and Prediction, in: Mathematical and Physical Sciences. volume 259, pp. 533–581.

Peng, D., Feng, L., Larson, K. M., & Hill, E. M. (2021). Measuring coastal absolute sea-level changes using GNSS interferometric reflectometry. Remote Sensing, 13(21). https://doi.org/10.3390/rs13214319

Peng, D., Hill, E. M., Li, L., Switzer, A. D., & Larson, K. M. (2019). Application of GNSS interferometric reflectometry for detecting storm surges. GPS Solutions, 23(2), 1–11. https://doi.org/10.1007/s10291-019-0838-y

Peng, Z. K., & Chu, F. L. (2004). Application of the wavelet transform in machine condition monitoring and fault diagnostics: A review with bibliography. Mechanical Systems and Signal Processing, 18(2), 199–221. https://doi.org/10.1016/S0888-3270(03)00075-X

Purnell, D. J., Gomez, N., Minarik, W., Porter, D., & Langston, G. (2021). Precise water level measurements using low-cost GNSS antenna arrays. Earth Surface Dynamics, 9(3), 673–685. https://doi.org/10.5194/esurf-9-673-2021

Purnell, D., Gomez, N., Chan, N. H., Strandberg, J., Holland, D. M., & Hobiger, T. (2020). Quantifying the Uncertainty in Ground-Based GNSS-Reflectometry Sea Level Measurements. IEEE Journal of Selected Topics in Applied Earth Observations and Remote Sensing, 13, 4419–4428. https://doi.org/10.1109/JSTARS.2020.3010413

Roesler, C., & Larson, K. M. (2018). Software tools for GNSS interferometric reflectometry (GNSS-IR). GPS Solutions, 22(3). https://doi.org/10.1007/s10291-018-0744-8

Roussel, N., Frappart, F., Ramillien, G., Darrozes, J., Desjardins, C., Gegout, P., Pérosanz, F., & Biancale, R. (2014). Simulations of direct and reflected wave trajectories for ground-based GNSS-R experiments. Geoscientific Model Development, 7(5), 2261–2279. https://doi.org/10.5194/gmd-7-2261-2014

Scargle, J. D. (1982). Statistical aspects of spectral analysis of unevenly spaced data. Astrophysical Journal, 263, 835–853.

Wan, W., Larson, K. M., Small, E. E., Chew, C. C., & Braun, J. J. (2015). Using geodetic GPS receivers to measure vegetation water content. GPS Solutions, 19(2), 237–248. https://doi.org/10.1007/s10291-014-0383-7

Wang, X., Zhang, Q., & Zhang, S. (2018a). Water levels measured with SNR using wavelet decomposition and Lomb–Scargle periodogram. GPS Solutions, 22(22). https://doi.org/10.1007/s10291-017-0684-8

Wang, X., Zhang, Q., & Zhang, S. (2018b). Azimuth selection for sea level measurements using geodetic GPS receivers. Advances in Space Research, 61(6), 1546–1557. https://doi.org/10.1016/j.asr.2018.01.002

Wang, X., Zhang, Q., & Zhang, S. (2019). Sea level estimation from SNR data of geodetic receivers using wavelet analysis. GPS Solutions, 23(6). https://doi.org/10.1007/s10291-018-0798-7